The Astrophysical Journal, 840:108 (13pp), 2017 May 10 https://doi.org/10.3847/1538-4357/aa6ff2

Gigahertz-peaked Spectra Pulsars and Thermal Absorption Model

J. Kijak[1], R. Basu[1], W. Lewandowski[1], K. Rożko[1], and M. Dembska[2]
[1] Janusz Gil Institute of Astronomy, University of Zielona Góra, ul. Z. Szafrana 2, PL-65-516 Zielona Góra, Poland; jkijak@astro.ia.uz.zgora.pl
[2] DLR Institute of Space Systems, Robert-Hooke-Str. 7 D-28359 Bremen, Germany
Received 2017 January 22; revised 2017 April 25; accepted 2017 April 25; published 2017 May 15

Abstract

We present the results of our radio interferometric observations of pulsars at 325 and 610 MHz using the Giant Metrewave Radio Telescope. We used the imaging method to estimate the flux densities of several pulsars at these radio frequencies. The analysis of the shapes of the pulsar spectra allowed us to identify five new gigahertz-peaked spectra (GPS) pulsars. Using the hypothesis that the spectral turnovers are caused by thermal free–free absorption in the interstellar medium, we modeled the spectra of all known objects of this kind. Using the model, we were able to put some observational constraints on the physical parameters of the absorbing matter, which allows us to distinguish between the possible sources of absorption. We also discuss the possible effects of the existence of GPS pulsars on future search surveys, showing that the optimal frequency range for finding such objects would be from a few GHz (for regular GPS sources) to possibly 10 GHz for pulsars and radio magnetars exhibiting very strong absorption.

Key words: ISM: general – ISM: supernova remnants – pulsars: general – stars: winds, outflows

1. Introduction

The radio spectra in pulsars, typically characterized by an inverse power law, have been important in understanding the nonthermal origin of radio emission in pulsars. In a majority of pulsars the spectral nature is described by a steep power-law function with an average spectral index of −1.8 (Maron et al. 2000). In recent years a new class of pulsars has been identified with a distinct spectral nature showing a turnover of around 1 GHz (Kijak et al. 2011b). These sources, classified as the gigahertz-peaked spectra (GPS) pulsars, exhibit the typical power-law spectrum at higher frequencies, but their observed flux decreases with frequency and the corresponding spectral index becomes positive at frequencies of <1 GHz. A systematic study was conducted by Kijak et al. (2007, 2011b, 2013) and Dembska et al. (2014, 2015a) where they reported nine pulsars and two magnetars that exhibited GPS characteristics. The GPS phenomenon appears to be associated with relatively young pulsars found in or around peculiar environments such as pulsar wind nebulae (PWNe), H II regions, etc. This motivated Kijak et al. (2011b) to suggest that the spectral turnover (∼1 GHz) is a result of the interaction of the radio emission with the pulsars' environments.

The unique binary system of PSR B1259−63 and the Be star LS 2883 provides a window into the GPS phenomenon (Kijak et al. 2011a). The spectrum of PSR B1259−63 at various orbital phases mimics the spectrum of a GPS pulsar. Kijak et al. (2011a) considered two mechanisms that might influence the observed radio emission: free–free absorption and cyclotron resonance. Most GPS pulsars have no companion, so there is no direct analogy between them and the binary system. However, the appearance of the GPS in isolated pulsars may be caused, like in the case of PSR B1259-63/LS 2883, by their peculiar environments (e.g., PWNe, supernova remnant [SNR] filaments). The interaction of the radio emission from pulsars with their environments was investigated in detail by Lewandowski et al. (2015c). They showed that the physical properties of certain environments suggest that thermal absorption can cause the observed spectra to turnover at GHz frequencies. The difference between the binary system and a typical GPS pulsar is that for PSR B1259−63 the intensity of the effect changes due to the variable amount of matter that the pulsar radiation has to pass through (Dembska et al. 2015b), whereas for the isolated pulsar the geometry of the absorber remains static, producing a stable, GPS-type spectrum. A similar approach was also used by Rajwade et al. (2016b) for a selected sample of six pulsars and by Basu et al. (2016) to explain the apparent variability of the spectra in PSR B1800−21.

The statistical studies of the past pulsar search surveys (see for example Bates et al. 2013) indicate that the pulsars exhibiting the GPS phenomenon can constitute up to 10% of the entire pulsar population. However, the relatively small sample of GPS pulsars (11 known cases) is understandable given that pulsar spectra are not well studied at low radio frequencies (below 1 GHz). The flux measurement becomes particularly challenging in pulsars with suspected GPS characteristics. The specialized environments around these pulsars imply that they generally have a relatively high (>200 pc cm^{-3}) dispersion measure (DM), and their profiles are significantly smeared by interstellar scattering; see Lewandowski et al. (2013, 2015a, 2015b) and Krishnakumar et al. (2015) for recent studies on scattering. As explained in Dembska et al. (2015a), the traditional flux measurement technique using single dish or phased-array telescopes is inadequate to measure the flux in highly scattered pulsars, leading to a gross underestimation of the pulsar flux. Interferometric imaging is the only method to securely measure the pulsar flux in such cases. In addition, Basu et al. (2016) carried out a detailed comparison between the two flux measurement schemes and demonstrated that interferometric imaging is a vastly superior technique to determine the pulsar flux.

The primary objectives of this paper are twofold. First, we have measured the flux in a large number of pulsars at low radio frequencies using the interferometric method. This is intended to extend the potential sample of GPS pulsars and also verify the GPS nature in a number of cases as a continuation of

the studies initiated in Kijak et al. (2011b, 2013) and Dembska et al. (2014, 2015a). Second, we have carried out detailed modeling using thermal free–free absorption following the suggestion of Kijak et al. (2011a, 2011b, 2013). The model fits were carried out for all pulsars exhibiting GPS characteristics, expanding the study of Lewandowski et al. (2015c) and Basu et al. (2016). We used the data-fitted models to estimate the physical properties of the absorbing electron gas—its density and temperature, and possible sizes of the absorber.

2. Observations and Data Analysis

We have conducted extensive observations using the Giant Metrewave Radio Telescope (GMRT) located near Pune, India. The GMRT consists of an array of 30 distinct dishes, each with a diameter of 45 m and spread out over a region of ∼27 km in a Y-shaped array. The GMRT operates mostly in the m wavelengths, between 150 MHz and 1.4 GHz, and is ideally suited to measure the pulsar flux at low radio frequencies and check their spectral shape. We used the 325 MHz and 610 MHz frequency bands for our studies and observed nine pulsars at 325 MHz and eight pulsars at 610 MHz, respectively. The data were recorded in the interferometric observing mode with each frequency band having a bandwidth of 33 MHz spread over 256 spectral channels. The 610 MHz observations were conducted between 2013 December and 2014 January, while the 325 MHz observations were carried out in 2015 January. Each source was observed for roughly one hour during each observing run at both frequencies. All observations were repeated twice, and the observing sessions were separated by a week to account for intrinsic flux variations as well as systematics.

The observations were carried out using standard interferometric schemes with strategically spaced calibrators interspersed with the sources. We recorded the flux calibrators 3C48 and 3C286 at the start and end of observations for around 8–10 minutes. In addition, a number of phase calibrators, spatially close to the pulsars, were selected and observed for 3–4 minutes every hour to account for the temporal gain variations in each antenna. The phase calibrators were also used to correct for fluctuations in the frequency band. During the 325 MHz observations two phase calibrators were used, 1714−252 and 1822−096, while the 610 MHz observations utilized five different phase calibrators: 1822−096, 1830−360, 1924+334, 2021+233, and 2047−026. The imaging analysis was carried out using the Astronomical Image Processing System, similar to Dembska et al. (2015a) and Basu et al. (2016). The flux scales of the calibrators 3C286 and 3C48 were set using the estimates of Perley & Butler (2013) and used to calculate the flux of the different phase calibrators (see Table 1). We reached noise levels of 0.2–0.5 mJy at 325 MHz, ensuring detections of all sources with flux in excess of 1.0–2.5 mJy (5σ detections). All the pulsars observed at 325 MHz could be detected in our observations; the only exception was PSR B1822−14, where the presence of a nearby strong source increased the noise levels and the pulsar was below the detection limit in the first observing session. The noise levels in the maps at 610 MHz were between 0.1 and 0.2 mJy, ensuring detection limits of between 0.5 and 1 mJy. However, we were only able to detect four of the seven sources at 610 MHz with the remaining pulsars (J1834−0812, J1856+0245, and J1916+0748) below the detection limit. The detailed results and implications of these measurements (shown in Table 2) are discussed in the subsequent sections.

Table 1
Observing Details

Obs. Date	Phase Calibrator	Flux (Jy)
	Day 1, 610 MHz	
2013 Dec 28, 29	1830−360	15.8 ± 1.0
2013 Dec 28, 29	1822−096	6.1 ± 0.4
2013 Dec 28, 29	1924+334	6.4 ± 0.5
2013 Dec 28, 29	2021+233	2.8 ± 0.2
2013 Dec 28, 29	2047−026	4.3 ± 0.3
	Day 2, 610 MHz	
2014 Jan 04, 07	1830−360	15.7 ± 0.9
2014 Jan 04, 07	1822−096	6.2 ± 0.4
2014 Jan 04, 07	2021+233	3.2 ± 0.3
2014 Jan 04, 07	2047−026	4.5 ± 0.3
	Day 1, 325 MHz	
2015 Jan 03, 04	1714−252	4.3 ± 0.2
2015 Jan 03, 04	1822−096	2.7 ± 0.3
	Day 2, 325 MHz	
2015 Jan 17, 18	1714−252	4.6 ± 0.3
2015 Jan 17, 18	1822−096	3.5 ± 0.3

2.1. The Thermal Absorption Model

In this section we present the basic tenets of the thermal free–free absorption to model the turnover in the spectra (Sieber 1973; Kijak et al. 2011a). To model the spectra we used the approach proposed by Lewandowski et al. (2015c) and used by Basu et al. (2016). In this model, the intrinsic pulsar spectrum is assumed to be a single power-law, and to estimate the optical depth we used an approximate formula for thermal free–free absorption (Rybicki & Lightman 1979; Wilson et al. 2009). The observed spectrum can be thus written as

$$S(\nu) = A\left(\frac{\nu}{\nu_0}\right)^{\alpha} e^{-B\,\nu^{-2.1}}, \quad (1)$$

where A is the intrinsic pulsar flux scaling factor (i.e., the flux density at the frequency of $\nu_0 = 10$ GHz), α is the intrinsic spectral index of the pulsar, and the frequency ν is in GHz. The optical depth τ was expressed by a product of the frequency dependent term and the frequency independent parameter $B = 0.08235 \times T_e^{-1.35}$ EM, where T_e is the electron temperature and EM is the emission measure (in pc cm^{-6}). The best fits to the measured spectra were obtained using the Levenberg–Marquardt least-squares algorithm. Compared to the earlier attempt at the modeling of the GPS pulsar spectra by Rajwade et al. (2016b), the model we use here is more adequate, since we use a full 3-parameter fit, while they performed a 2-parameter fit using high-frequency flux measurements as an "anchor point" instead of fitting for the intrinsic pulsar flux amplitude A.

Table 3 shows the best fit values for parameters A, B, and α, along with the normalized χ^2 and the resulting peak frequency, i.e., the observing frequency at which the model reaches maximum flux. We also included the values of the reduced χ^2 for a single power-law fit for comparison, and as one can see for all pulsars all but one the thermal absorption model provides a significantly better fit to the spectra. The

Table 2
Flux Density Measurements (S_1, S_2) Resulting from the Observations in Two Separate Observing Sessions at 325 MHz and 610 MHz, Respectively, Along with the Uncertainties that Include Calibration Errors, the rms Noise in the Maps, and Fitting Error

Pulsar	S_1 (mJy)	S_2 (mJy)	$\langle S \rangle$ (mJy)
	325 MHz		
B1641−45	140.2 ± 7.9	152.1 ± 8.5	145.7 ± 8.2
J1723−3659	1.1 ± 0.3	1.4 ± 0.3	1.3 ± 0.3
B1822−14	<2.5	2.4 ± 0.4	2.4 ± 0.4
B1823−13	1.2 ± 0.3	1.3 ± 0.2	1.3 ± 0.3
B1832−06	13.6 ± 0.9	16.0 ± 1.0	14.7 ± 0.9
J1835−1020	1.6 ± 0.4	2.4 ± 0.3	2.1 ± 0.3
J1841−0345	1.3 ± 0.3	2.3 ± 0.6	1.5 ± 0.4
J1852−0635	1.3 ± 0.3	1.8 ± 0.2	1.6 ± 0.2
J1901+0510	1.0 ± 0.3	1.2 ± 0.3	1.1 ± 0.3
	610 MHz		
J1834−0731	3.4 ± 0.5	4.5 ± 0.5	4.0 ± 0.5
J1834−0812	<0.85	<0.95	···
J1852−0635	5.2 ± 0.4	5.2 ± 0.4	5.2 ± 0.4
J1856+0245	<0.75	<0.85	···
B1904+06	2.8 ± 0.3	3.0 ± 0.3	2.9 ± 0.3
J1916+0748	<0.45	<0.45	···
J2007+2722	1.6 ± 0.3	1.7 ± 0.2	1.7 ± 0.3

Note. $\langle S \rangle$ denotes the weighted mean of all results and its uncertainty for a given pulsar.

uncertainties of the fitted parameters were obtained using three-dimensional χ^2 mapping. The dashed lines in the spectra plots shown in the next section represent the envelopes of all the models that lie within a 1σ boundary of a best-fit model for the given spectrum.[3]

3. Results

Table 2 shows the results of our flux density measurements for individual observations at both frequencies as well as for the average value. As mentioned in the previous section, the pulsars J1834−0812, J1856+0245, and J1916+0748 were below our detection limit at 610 MHz. Using the newly acquired data and the previously published flux measurements (see figure captions) we constructed the spectra for all pulsars that either exhibit GPS behavior or had been suspected of doing so before our recent observations. The spectra are shown in Figures 1–4, and the new measurements are denoted by the filled symbols. The spectra were divided into four groups: the new GPS pulsars (Figure 1), the objects for which the GPS feature was confirmed earlier (Figure 2), the spectra that resemble a simple power-law (Figure 3; these pulsars were usually suspected or previously claimed to show a high frequency turnover), and finally the spectra of two pulsars that still require further investigation (Figure 4), which we consider to be promising GPS candidates. In all of these figures except the last one we also show the results of spectral modeling fits.

In our analysis we omitted some of the archival measurements for pulsars B1822−14 and B1823−13 that were published by Lorimer et al. (1995). These measurements were indicated by the authors of that work as suspicious and possibly affected by interstellar scattering. As we mentioned in the Introduction, and also discussed previously in Kijak et al. (2011b) and Dembska et al. (2015a), that may lead to a severe underestimation of the received flux density when measured by a standard pulse profile–based method. The theoretical aspects of the influence of interstellar scattering on the observed pulsar flux were also recently discussed by Geyer & Karastergiou (2016). This calls for caution when using archival (or catalog) flux density measurements, especially at low frequencies, where the effects of scattering-induced flux underestimation will be strongest.

3.1. New and Confirmed GPS Pulsars

Figure 1 shows the spectra of five pulsars for which the GPS effect is presented for the first time. These objects are characterized by relatively high DM values (>190 pc cm^{-3}), except for PSR J1841−0345, which has DM = 56 pc cm^{-3}. Most of the pulsars are relatively young, $\tau < 10^6$ year (see Table 4; the basic pulsar parameters were taken from the Australia Telescope National Facility [ATNF] Catalog.[4])

For pulsars J1723−3659, J1835−1020, and J1901+0510 our new measurements were only the third in their respective spectra. Having three data points makes it impossible to model the spectrum with three parameters. In the case of these three pulsars, we have limited the number of fitted parameters by an additional assumption that the pulsar's intrinsic spectrum has a spectral index of −1.8 (the average value for the nonrecycled pulsar population; see Maron et al. 2000), and we estimate only A and B parameters from the fits.

Figure 2 presents the spectra of four objects that were classified as GPS pulsars by Kijak et al. (2011a, 2011b), Dembska et al. (2014), and Allen et al. (2013). The objects were included in our sample to confirm the shape of the spectra and put better constraints on the thermal absorption model by adding new measurements at low observing frequencies (where the free–free absorption manifests itself the strongest). In all four cases the new measurements confirm the earlier claims of high frequency turnovers.

3.2. Objects with Typical Spectra and GPS Candidate Pulsars

The pulsars whose spectra are shown in Figure 3 were suspected to show the GPS phenomenon in our earlier studies and hence were included in our observing sample. However, our new measurements (together with the previously published flux density values) clearly show that pulsars B1832−06, J1834−0731, and B1904+06 exhibit regular power-law spectra down to 300 MHz.

Figure 4 presents the spectra of two pulsars we attempted to measure in our observations, but we only obtained upper limits for their flux density at 610 MHz. We still believe that these objects are good candidates for GPS pulsars. PSR J1834−0812 exhibits a very high DM (DM = 1020 pc cm^{-3}). For PSR J1916+0748, the upper limit for the flux density clearly suggests a positive spectral index; however, we cannot explain why our limit is lower than the earlier measured flux at 400 MHz.

[3] For a given spectrum, all the models that agree with the best fit to the 1σ level will in their entirety lie within the envelope.

[4] Available at http://www.atnf.csiro.au/people/pulsar/psrcat/; Manchester et al. (2005).

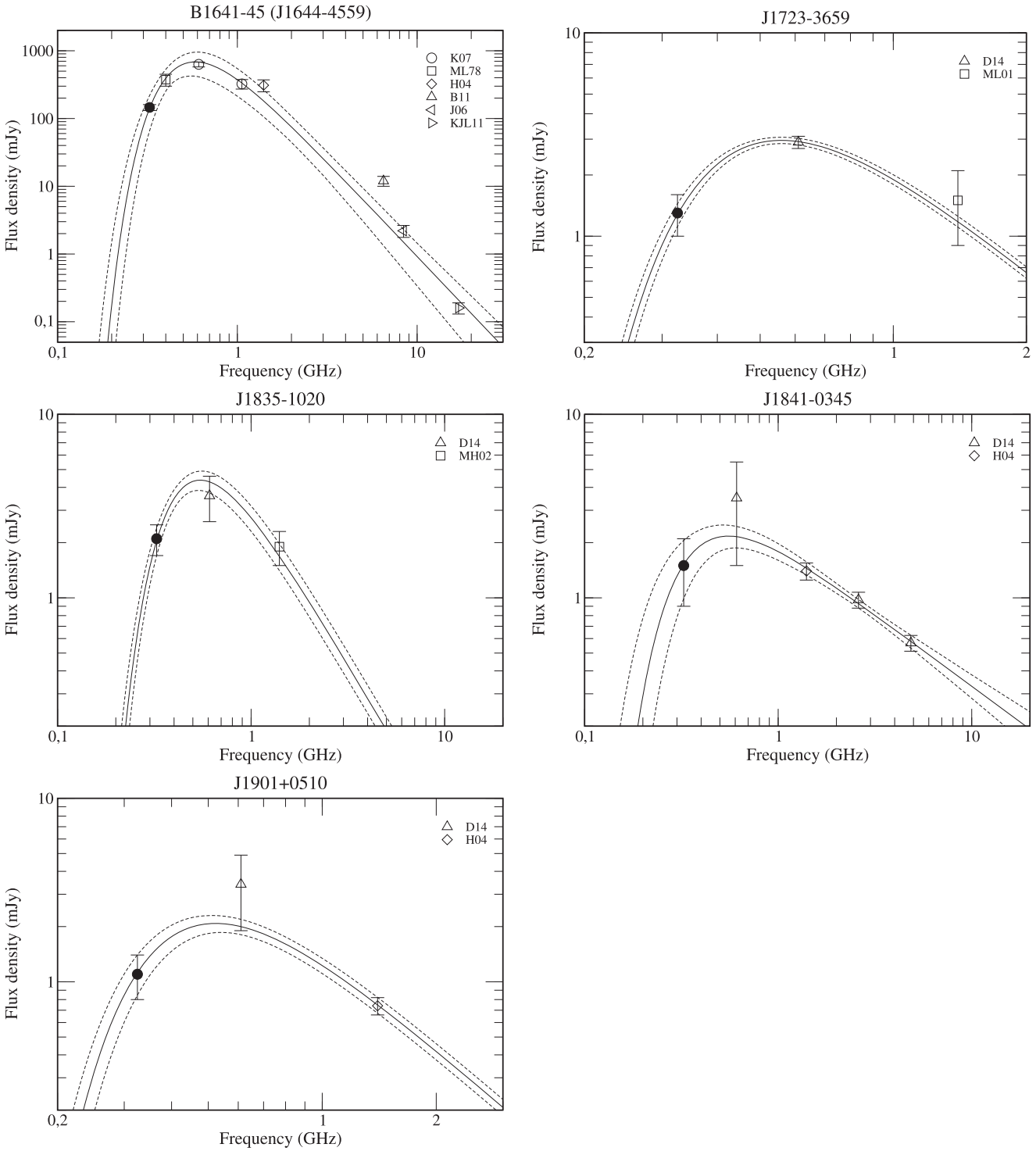

Figure 1. New GPS pulsars. The empty circles show flux density from the literature (see References). Our measurements are denoted by filled circles. Other values were taken from the literature: K07—Kijak et al. (2007), ML78—Manchester et al. (1978), H04—Hobbs et al. (2004), B11—Bates et al. (2011), J06—Johnston et al. (2006), KLJ11—Keith et al. (2011), D14—Dembska et al. (2014), ML01—Manchester et al. (2001), and MH02—Morris et al. (2002). The solid line represents the thermal absorption model fit for the observed data with a 1σ envelope (dashed lines). The fitted parameters are presented in Table 3.

3.3. Radio Magnetars and Other GPS Pulsars

Figures 5 and 6 present the spectra of the GPS pulsars and radio magnetars that were published earlier (Kijak et al. 2007, 2011a, 2011b, 2013). We did not add any new data points to these spectra; however, for completeness, we decided to apply the thermal absorption model to these spectra as well. The results of our fits are included in Table 3. In the case of PSR B1054−62 there are some results that allow for a power-law spectrum to within a 1σ level. This is indicated by the shapes of the 1σ envelopes and that the uncertainty in the B parameter (see Table 3) extends down to include the value of $B = 0$ within the 1σ level, which means no absorption. Similar is the case of PSR J1809−1917, the only pulsar in Table 3, for which the reduced χ^2 from a power-law fit is lower than that

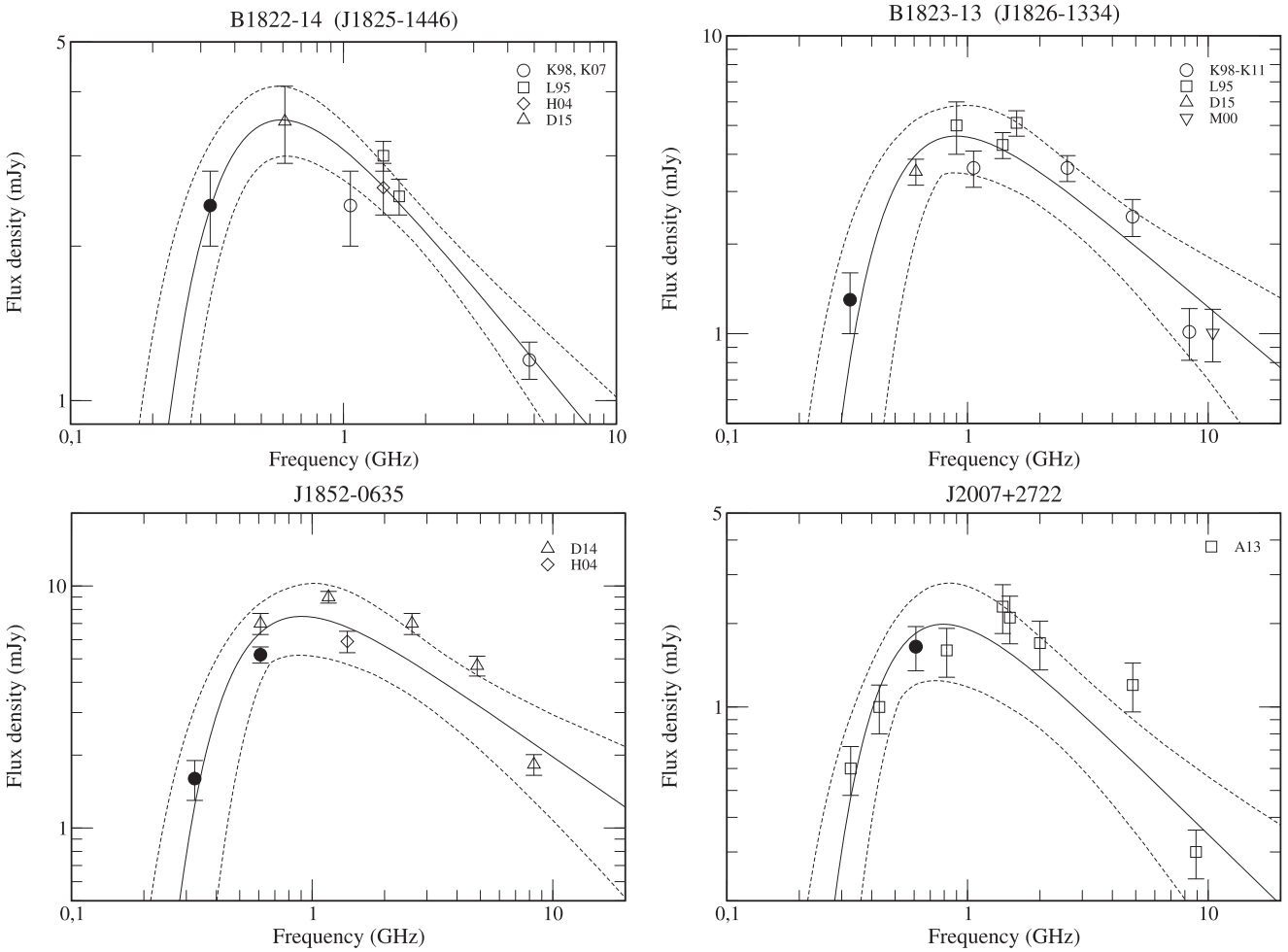

Figure 2. Four confirmed GPS pulsars. The spectral fits and errors during fitting are shown as solid and broken lines, respectively. The fitted parameters and the physical parameters of the absorbing medium are presented in Tables 3 and 4, respectively (see also Figure 1). Filled circles represent our new measurements. The remaining flux values were taken from the literature: K98-K11—Kijak et al. (1998, 2007, 2011b), Kijak & Maron (2004), L95—Lorimer et al. (1995), D15—Dembska et al. (2015a), M00—Maron et al. (2000), and A13—Allen et al. (2013); see also Figure 1. For PSRs B1822−14 and B1823−13 we omitted the flux measurements at 610 MHz from Lorimer et al. (1995) since they were most likely heavily affected by scattering effects—see the discussion in the Results section.

for the thermal absorption fit. Compared to the spectrum that was shown earlier in Kijak et al. (2011b), we added a measurement from Bates et al. (2011) at 6.5 GHz. The large discrepancy between this measurement and our previous 5 GHz measurement causes the fit to be less conclusive. This is because in our modeling the high-frequency part of the spectrum is primarily used to ascertain the slope of the intrinsic pulsar spectrum. Hence the discrepancy between two high frequency measurements translates to large uncertainties, as we cannot exclude the possibility that the intrinsic spectrum is relatively flat. We decided, however, to include this pulsar as a GPS source—the low-frequency part of the spectrum clearly indicates a turnover, as the 1170 MHz flux is almost 2.5 times smaller than the 1.4 GHz flux.

Lewandowski et al. (2015c) used the thermal absorption model to explain the observed GPS-like evolution of the Sgr A* radio magnetar spectrum (PSR J1745−2900). Here we show the spectra of another two radio magnetars that were pointed out by Kijak et al. (2013) to show the GPS characteristics. The results of our modeling clearly show that the high frequency turnovers in the spectra are undeniable, since—as it is indicated by the shape of the 1σ envelope—no single power-law model will agree with our results to within a 1σ uncertainty.

3.4. Break or Turnover in the Spectrum of PSR B1828−11

In Figure 7 we present the spectrum of PSR B1828−11. This pulsar was previously studied by Kijak et al. (2011b) and was classified as a flat-normal, or in other words a broken spectrum, with the spectral index of −2.4 in the high-frequency range, and 0.5 in the low-frequency range, below 1.2 GHz. Despite having no new observations for the source, we decided to apply our thermal absorption model to its spectrum (see Table 3 for the results of our fit). We believe that the results of our modeling show that the broken spectra of pulsars can be, at least in some of the cases, explained with the absorption model. The lack of a spectral turnover in such a case may be the result of the limited range of frequencies over which the pulsar flux density measurements were taken. To test that hypothesis, detailed observations at lower frequencies are necessary.

4. Discussion

The interferometric imaging technique is a much superior technique to estimate the pulsar flux (see Basu et al. 2016) and

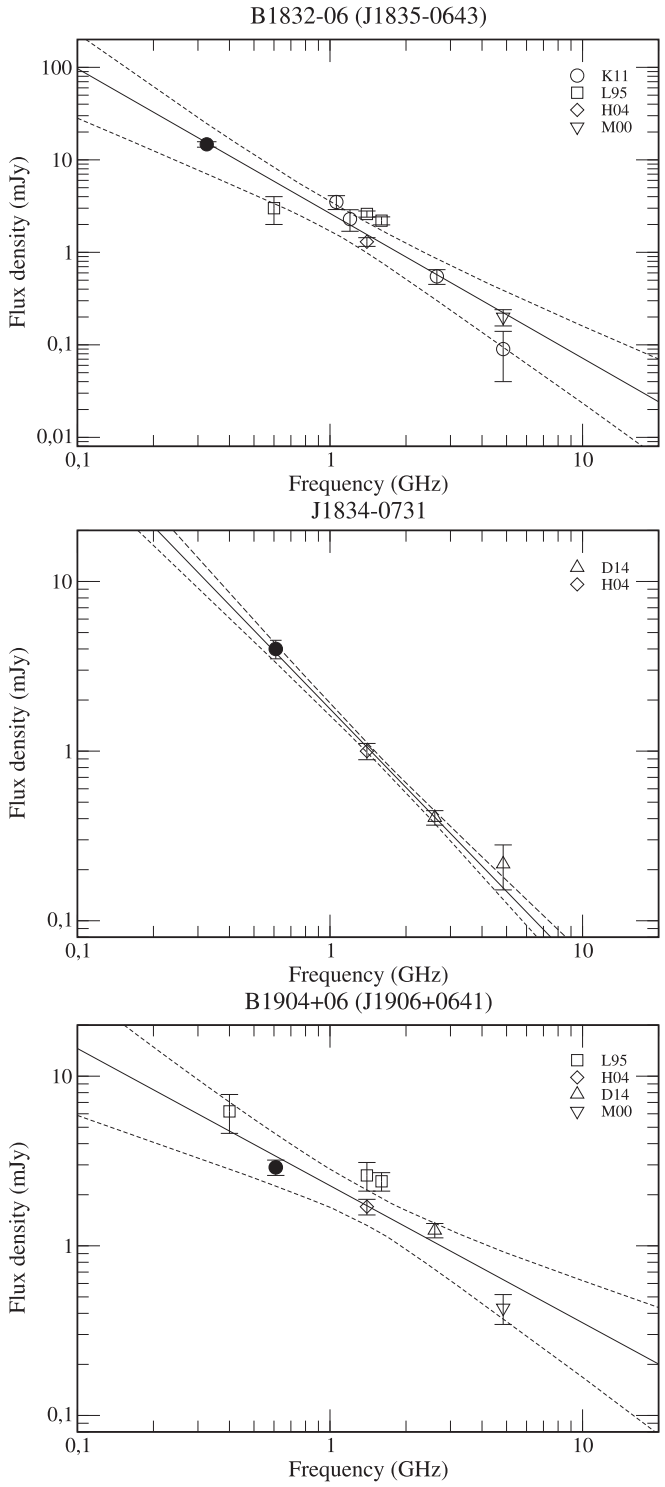

Figure 3. The typical pulsar spectra have been modeled using a simple power-law model. Filled circles represent our new measurements, and the remaining flux values were taken from the literature; the acronyms are explained in the previous figures. The solid line represents the model fit for the observed data with a 1σ envelope (dashed lines). The PSRs B1832−06, J1834−0731, and B1904+06 have the dispersion measures 472, 295, and 472 pc cm^{-3}, respectively, and are middle-aged objects of 120, 140, and 1980 kyr, respectively (see also Figure 1).

provides the only means to estimate the flux of pulsars that are affected by scattering (see discussion in Dembska et al. 2015a). Given the robustness of our flux measurements, we were able to estimate the low-frequency spectra in several pulsars and found five new cases of GPS: PSR B1641−45, PSR J1723−3659, PSR J1835−1020, PSR J1841−0345, and PSR J1901+0510. In addition, we also verified the GPS phenomenon in another four pulsars. The spectral turnover in 15 GPS pulsars was successfully explained using the thermal absorption model (see Table 4). In the remainder of this section we explore the physical implications of these results.

The spectra of six GPS pulsars were previously modeled using the thermal absorption hypothesis by Rajwade et al. (2016b). Their models were using our data from Kijak et al. (2007, 2011b) and Dembska et al. (2014). For five of these sources we are showing a model based on spectra in a wider frequency range as we add new flux density measurements mainly at low frequencies. This, in conjunction with using a full three-parameter model, allows us to obtain much more reliable estimates of the absorbers' physical parameters.

4.1. Thermal Absorption as the Source of Spectral Turnovers

The idea of thermal free–free absorption as the source of the low-frequency spectral turnovers in pulsars was first proposed by Sieber (1973) and was proposed to explain the GPS spectra of pulsars and magnetars by Kijak et al. (2011a, 2013). Lewandowski et al. (2015c) showed that indeed the peculiar environments of some pulsars may provide sufficient amounts of absorption to cause the spectra to turn over at GHz frequencies. Until now we were aware of the low-frequency turnovers (around 100 MHz) and of the GPS in which the peak frequency was reported to be around 1 GHz (see Kijak et al. 2011a, 2011b, 2013; Dembska et al. 2014, 2015a). However, the results we present here show rather a continuous range of peak frequencies (see Table 3), not merely bimodal frequencies. In addition, owing to the use of an actual physical model instead of purely morphological attempts (using for example Kuzmin & Losovsky 2000; log-parabolic fits), the peak frequencies we obtained are lower than the values estimated earlier. This is to be expected, since the spectral profile of the absorption will be always asymmetric, with the peak shifted toward lower frequencies.

The fact that the peak frequencies in the pulsar spectra affected by thermal absorption cover a wide range of values should come as no surprise, since in reality both the intersellar medium (ISM) and the immediate pulsar surroundings can show a wide and roughly continuous range of physical parameters relevant to this phenomenon. Depending on the amount of absorption, which in itself is bound to the physical properties of the absorbing matter (electron density, temperature and its extent along the line of sight), one can expect that different configurations will cause the spectra to peak at different frequencies—below 300 MHz for pure ISM and around 1 GHz for pulsars obscured by dense SNR filaments. In addition, the entire range between these two possibilities should be covered by ionized clouds—regions that have electron densities higher than neutral ISM but not as high as the compact clumps of matter in SNRs.

4.2. The Absorber's Physical Parameters

Following Lewandowski et al. (2015c) and Rajwade et al. (2016b), we point out that the free electrons in the ISM contribute to both the observed dispersion of the pulsar signal and the absorption. In the case of the dispersion effect, the contribution from any region of space is proportional to its

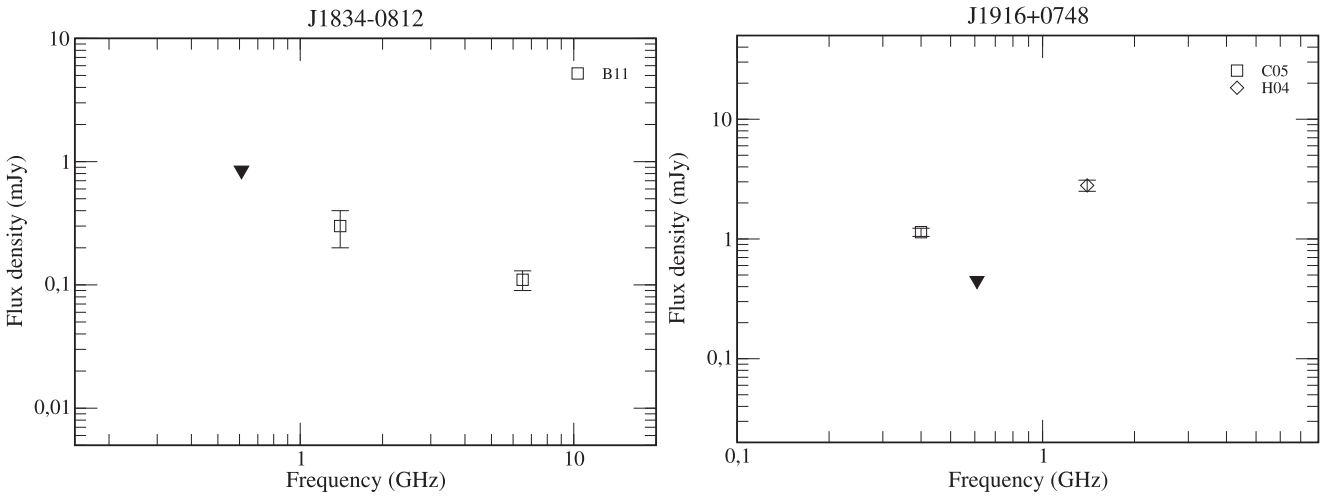

Figure 4. Candidates for GPS pulsars. The inverted triangles show the upper limits from our observations, C05 was taken from Champion et al. (2005), and the remaining flux values were taken from the literature; the acronyms are explained in the previous figures. PSRs J1834−0812 and J1916+0748 have a characteristic age of 781 and 802 kyr, respectively, and DM = 1020 and 304 pc cm^{-3}, respectively.

electron density n_e, but the same region contributes to the optical depth as its n_e^2. Using our assumption of a dense uniform region as the source of the absorption, we can estimate its EM along the line of sight to be EM $= n_e^2 \times s$, where s is the width of the absorber. However, this absorber will also contribute to the pulsar's DM, providing $\Delta \mathrm{DM} = n_e \times s$.

Our best model fits provide parameter B, which is dependent on the temperature of the electrons and the EM. Using the above, it can be written as $B = 0.08235 \times T_e^{-1.35} \times n_e^2 \times s$, which gives us the first equation binding these three parameters. The DM provides the second equation, but since the DM's dependence on the electron density is not as steep as in the case of thermal absorption, one cannot negate the DM contribution from the general ISM (i.e., the region outside of the absorber). Obviously, without additional information about the electron density and the size of the absorbing region, we cannot reliably estimate the fraction of the total observed DM that comes from the absorber. Following Rajwade et al. (2016b) and Basu et al. (2016), for the purposes of our calculations we assumed that for the pulsars exhibiting the GPS phenomenon—hence the ones that have a well-defined absorber along their line of sight—the contribution to the DM from the absorber is equal to half of the observed DM value. This allows us to write the second equation concerning the physical parameters of the absorber: $0.5\ \mathrm{DM} = n_e \times s$.

Since we have only two equations and three free parameters (s, n_e, and T_e), it is impossible to solve for the values of the parameters without additional information about at least one of them or without additional assumptions. In the case of pulsar observations the additional information is usually not available, as it is extremely hard to identify the actual absorber, or—in the case of known PWNe—to extract the physical parameters of the region that will contribute to radio wave absorption. Therefore, following Basu et al. (2016), we decided to continue our analysis for three distinct categories of possible absorbers:

1. dense filaments in an SNR with typical $s = 0.1$ pc,
2. comet-shaped tail in a PWN with $s = 1.0$ pc, and
3. H II region with $s = 10$ pc.

Table 4, in addition to basic and relevant pulsar parameters (i.e., DM, characteristic age, and possible associations) shows the results of our calculations for the physical properties of the absorbing region using the three cases described above: i.e., for every pulsar the electron density and temperature were calculated for hypothetical absorbers with a physical width of 0.1, 1.0, and 10 parsec. Based on this information one can attempt to identify the type of absorbing region by excluding the unphysical or unlikely parameter combinations as explored in Section 4.3.

4.3. Constraints on Possible Astrophysical Absorbers

Lewandowski et al. (2015c) pointed out that it is extremely difficult to estimate electron densities and temperatures in the pulsar surroundings, using observational data that are, as a result, extremely rare. In the case of the GPS pulsars identified so far such data are not available. In addition, the situation is even more futile in the case of pulsar spectral observations, since from such studies one cannot ascertain the geometry of the absorber: its actual location and size (i.e., its extent along the line of sight) remain unknown. In fact, the location of the absorber is completely irrelevant to the amount of the observed absorption. We can only assume that the absorption happens in the vicinity of the pulsar, since pulsars (especially the young ones) are often located in environments with relatively high electron density.

For the above reasons we are at the moment unable to predict the actual physical parameters of the absorbing matter that causes the turnover in pulsar spectra. However, we can put some observational constraints on these absorbers. This allows us at least to some degree to distinguish between the different kinds of astrophysical sources of absorption and point out the most likely case or at the least to exclude the nonviable possibilities.

In Table 4, we present the results of our calculations of the physical properties of the absorbers that would cause the observed amount of absorption for each of the GPS pulsars. For each of the sources, we calculated the required electron density and temperature assuming three different sizes of the hypothetical absorber. These represent an absorption in an H II region (10 pc in size), a shell of a PWN, or a small H II region (1 pc) and a dense SNR filament (0.1 pc). The corresponding derived values of electron density and

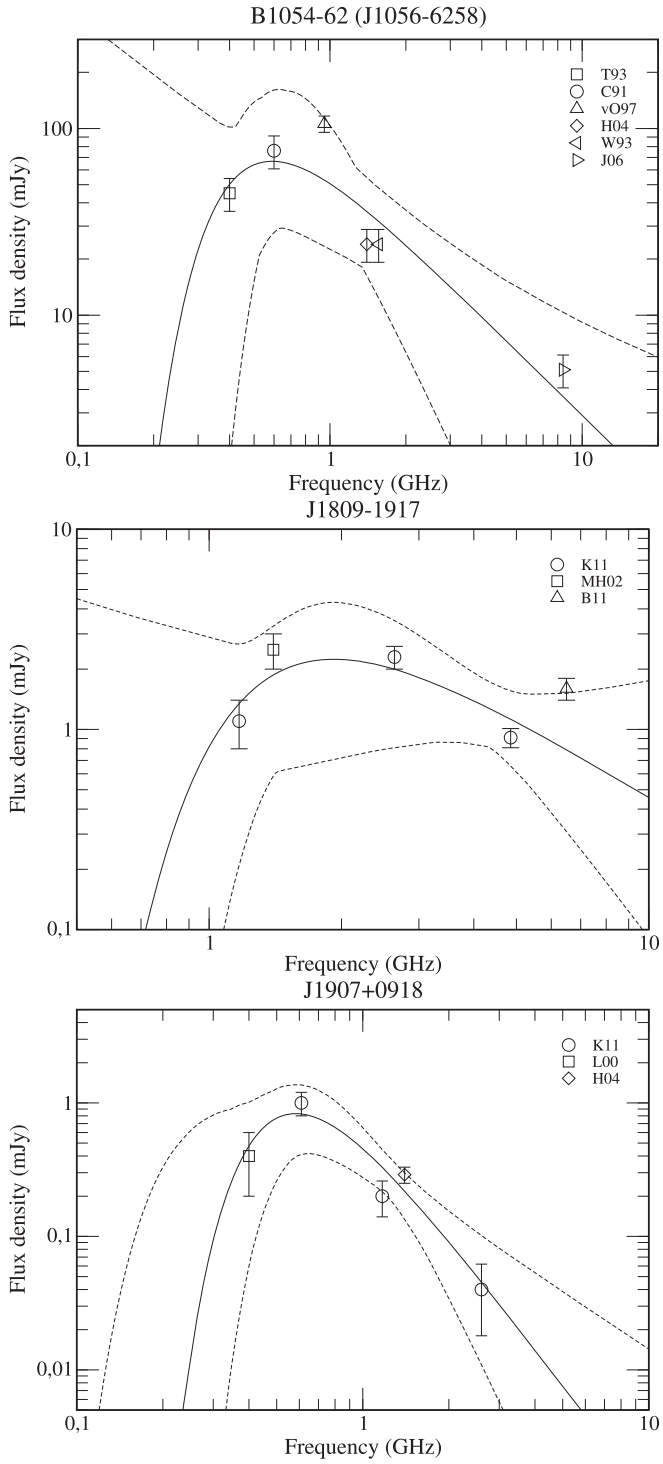

Figure 5. Other GPS pulsars with the absorption model fits. Data are taken from T93—Taylor et al. (1993), C91—Costa et al. (1991), vO97—van Ommen et al. (1997), W93—Wu et al. (1993), and L00—Lorimer & Xilouris (2000), and the remaining acronyms are explained in the previous figures.

temperature can be used to estimate the likelihood of a particular type of absorber being the reason for the GPS behavior. For example, in virtually all the cases presented in Table 4, the assumption of the H II absorber yields somewhat realistic values of the electron density, up to a few tens of electrons per cubic centimeter; however, the corresponding electron temperatures are extremely low (below 100 K), which is unphysical for this type of ionized region (typical electron temperatures in H II regions are on the order of a few thousand kelvins). Therefore we can confidently exclude them as possible absorbers.

In general, we believe that our calculations clearly show that extended H II regions are the most unlikely causes for the appearance of the GPS spectra. The high electron temperature in such regions causes the ISM to be more transparent. To provide enough absorption in such a case, the electron density would have to be much higher. While the high value of density on its own is not an issue, since some of the H II regions exhibit densities of up to 10^5 particles per cm^3, one has to realize that the same region would also provide the dispersion of the pulsar signal. The value of the observed DM is easy to calculate: a 10 pc region with an electron density of 1000 particles per cm^3 would provide 10,000 pc cm^{-3} of dispersion, making the pulsar very unlikely, or even impossible, to be discovered in a regular pulsar survey (even provided that the survey would be conducted at a high frequency, where thermal absorption would not play a significant role).

As for the other types of absorbers, the interpretation is usually not as straightforward, since these kinds of pulsar environments can exhibit a range of physical parameters. As Lewandowski et al. (2015c) pointed out, the dense filaments in an SNR can be dense enough (up to a few thousand particles per cubic centimeter) that even when considering their high temperature (up to a few thousand kelvins), they still provide enough absorption to cause spectral turnover at GHz frequencies while being only a fraction of a parsec in size. Looking at the data in Table 4, a number of pulsars seem to fit the criteria: for example, PSR B1054−62 ($n_e = 1601$ cm^{-3}, $T_e = 5080$ K), PSR B1822−14 ($n_e = 1785$ cm^{-3}, $T_e = 10100$ K), and several others. Obviously, not all of the GPS pulsars listed in the table that would fit the SNR filament scenario were actually observed within an SNR; however, this can be caused by the fact that the distant remnants are especially difficult to detect. In addition, one has to remember that the absorber does not have to be physically or evolutionarily connected to the remnant—just as in the case of PSR B1800−21, studied by Basu et al. (2016), an object whose line of sight apparently crosses an unrelated W30 remnant nebula.

Distinguishing between absorption in a dense filament and absorption in a shell (or rather "tail") of a PWN may be more difficult. Lewandowski et al. (2015c) showed that the measurements of the temperatures and densities in comet-shaped PWNe are very sparse, at least when it comes to those parts of the nebulae that could possibly provide free–free absorption in the radio regime. They also show that if one considers densities of the order of a few hundred particles per cm^3, then for a roughly 1pc size of the absorber in the PWN tail one would need temperatures as low as few hundred kelvins to provide significant absorption at GHz frequencies. Based on the data we show in Table 4, several pulsars would qualify in this category, such as PSR B1641−45 ($n_e = 239$ cm^{-3}, $T_e = 983$ K). However, for these sources the SNR filament scenario also provides reasonable parameters, making it extremely difficult to decide which of these two possibilities we are dealing with for a particular pulsar. To solve this one would need some additional observations, like the detection of a PWN, or measurements of the associated/coincident SNR. However, in the case of the confirmed GPS pulsars such observations are not available, and even in the cases with a

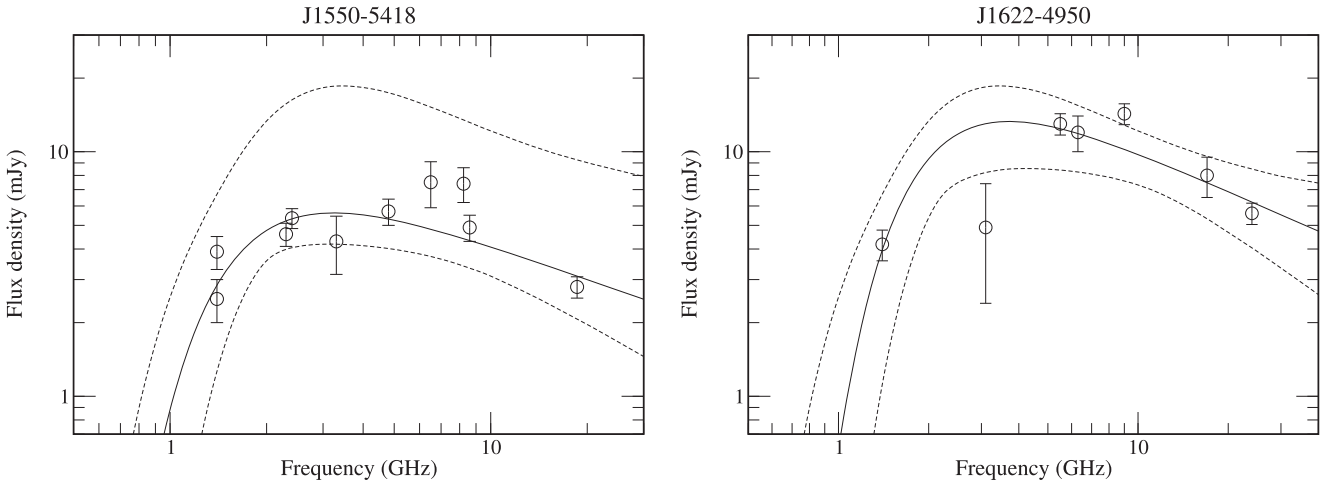

Figure 6. Absorption model fits for the observed data in two radio magnetars (see Kijak et al. 2013). Data are taken from Camilo et al. (2007, 2008) and Bates et al. (2011) for PSR J1550−5418 and from Levin et al. (2010, 2012), Keith et al. (2011), and Anderson et al. (2012) for PSR J1622−4950.

confirmation of a PWN or an SNR the data are not detailed enough to provide information that would allow us to estimate the parameters relevant to the thermal absorption of radio waves. Finally, since the effect of absorption in our model does not depend on the actual location of the absorber, we expect that in some cases we may see the pulsars through absorbers that are not in their immediate vicinity, which makes the interpretation even harder; the possibility of multiple absorbers (with different physical parameters) cannot also be excluded.

4.4. Finding GPS Pulsars in Future Surveys

Based on the values of peak frequency we obtained (see ν_p in Table 3), we created a histogram of the peak frequency distribution, which is shown in Figure 8. To create the histogram we included all the pulsars and radio magnetars presented in this work, as well as the data from the binary pulsar B1259−63 (Kijak et al. 2011a; we used the lowest peak frequency found there, 1.6 GHz), the Galactic center radio magnetar J1745−2900 (Pennucci et al. 2015; the peak frequency is slightly larger than 2 GHz), and PSR B1800−21 (Basu et al. 2016). While the statistics are still small, in looking at the histogram one can note a difference between the regular GPS pulsars and the peak frequencies in the spectra of radio magnetars. This may be at least partially explained by the differences in the methods of discovery. The radio magnetars are always found by targeted searches following an X-ray outburst of the source and the X-ray data often provide the rotational period, which significantly narrows the parameter space that needs to be searched to find the radio counterpart.

On the other hand, finding a GPS pulsar with a peak frequency higher than, say, 1.5 GHz will be difficult. An optimal frequency range for a GPS pulsar search is definitely much higher than its peak frequency. For example, if $\nu_{0.9}$ is the frequency at which one would see 90% of the pulsar's flux, then using simple algebra one can show that $\nu_{0.9}/\nu_p \approx \sqrt{4.5 \times \alpha}$ (where α is the intrinsic pulsar spectral index). For a typical pulsar ($\alpha \approx 2$) this means that only in the frequency range greater than times the peak frequency, the observer receives almost all of the pulsar intrinsic flux, making this range optimal for detection. This would explain the lack of regular pulsars with ν_p above 2 GHz, since the search for such sources would be most effective at frequencies higher than 6 GHz. There have only been a few limited attempts to search for pulsars in this range, e.g., the Parkes Methanol Multibeam Survey (Bates et al. 2011). One of the main reasons why such searches are not attempted more often is that blind surveys at such high frequencies are extremely time consuming. This is due to the decreased telescope beam size, which in turn decreases the Galaxy volume that may be searched in a given time. In addition, GPS pulsars with such a high absorption would also most likely exhibit high values of DM, which would happen regardless of their distance since the absorption and its associated high DM contribution are most probably local to the pulsar. However, the possibility of a large DM value may significantly increase the parameter space that has to be searched since the dispersion smearing is inversely proportional to the observing frequency squared. This may not be a big issue for such high-frequency searches.

Rajwade et al. (2016a) recently published a detailed study of past and proposed high-frequency pulsar surveys, calculating the expected discovery probabilities while taking into account the effects of thermal free–free absorption and scattering. They showed that the optimal frequency range for finding pulsars in the central regions of the Milky Way would be 9 to 13 GHz, and they claimed that the main limiting factor in this case will be the interstellar scattering, not absorption. However, in their calculation of thermal absorption they used an EM of 5×10^5 pc cm^{-6} for the Galactic center pulsars. As we show in Table 4, in some scenarios the GPS spectrum may be explained by regions with an EM exceeding 10^6 pc cm^{-6} (see the radio magnetars in the 0.1 pc absorber case), which means that for very dense environments the thermal absorption may play a much stronger role in the probability of detection than Rajwade et al. (2016a) used for the proposed Galactic center surveys.

For the above reasons we believe that there is still a high chance that we can discover GPS pulsars in some of the less studied PWNe or SNRs by means of targeted searches at frequencies close to and above 10 GHz. Additional targets for such searches may be the unresolved X-ray sources that show characteristics of a PWN (e.g., with regard to their spectra). There is also a chance that a number of GPS pulsars still remains undetected in the larger/more dense/cooler H II regions and possibly in the center of the Milky Way. Blind surveys performed at higher frequencies may also yield

Table 3
Parameters Obtained by Modeling of the Spectrum of Pulsars (see details in Paragraph 3.1)

PSR	A	B	α	$\nu_{\rm p}$ (GHz)	χ^2	$\chi^2_{\rm PL}$	
B1054−62	$2.9^{+6.2}_{-2.8}$	$0.21^{+1.01}_{-0.21}$	$-1.33^{+0.78}_{-2.34}$	0.59	12.21	14.1	5
J1550−5418	$4.16^{+1.02}_{-0.99}$	$2.6^{+2.7}_{-1.9}$	$-0.46^{+0.32}_{-0.34}$	3.23	2.54	6.38	6
J1622−4950	10.1 ± 2.6	$4.1^{+3.2}_{-2.3}$	-0.54 ± 0.37	3.73	5.09	12.9	6
B1641−45	$0.92^{+0.53}_{-0.58}$	0.43 ± 0.11	$-2.79^{+0.28}_{-0.40}$	0.58	6.02	32.8	1
J1723−3659	$0.039^{+0.003}_{-0.002}$	$0.252^{+0.018}_{-0.016}$	−1.8	0.56	0.30	17.6	1
J1809−1917	$0.47^{+1.28}_{-0.37}$	$2.52^{+4.94}_{-2.52}$	-1.34 ± 1.8	1.93	12.1	9.9	5
B1822−14	$0.77^{+0.25}_{-0.21}$	$0.104^{+0.055}_{-0.047}$	$-0.65^{+0.17}_{-0.19}$	0.60	1.03	5.1	2
B1823−13	$1.23^{+0.58}_{-0.53}$	$0.26^{+0.42}_{-0.14}$	$-0.68^{+0.26}_{-0.42}$	0.90	3.21	17.7	2
B1828−11[a]	$0.010^{+0.008}_{-0.006}$	0.85 ± 0.24	$-2.62^{+0.37}_{-0.48}$	0.83	1.74	17.3	7
B1832−06	$0.072^{+0.076}_{-0.044}$	⋯	-1.57 ± 0.26	⋯	⋯	7.03	3
J1834−0731	$0.051^{+0.002}_{-0.003}$	⋯	$-1.54^{+0.13}_{-0.09}$	⋯	⋯	0.66	3
J1835−1020	$0.055^{+0.010}_{-0.009}$	$0.241^{+0.026}_{-0.025}$	−1.8	0.55	0.78	2.6	1
J1841−0345	$0.331^{+0.051}_{-0.047}$	$0.108^{+0.049}_{-0.040}$	-0.78 ± 0.11	0.55	0.41	2.4	1
J1852−0635	$1.97^{+0.97}_{-0.89}$	$0.27^{+0.37}_{-0.14}$	$-0.69^{+0.30}_{-0.44}$	0.90	7.54	36.0	2
J1901+0510	$0.024^{+0.0026}_{-0.0025}$	$0.22^{+0.03}_{-0.02}$	−1.8	0.52	0.89	15.1	1
B1904+06	$0.36^{+0.25}_{-0.17}$	⋯	-0.79 ± 0.23	⋯	⋯	5.35	3
J1907+0918	$0.0011^{+0.0132}_{-0.0011}$	$0.43^{+0.65}_{-0.34}$	$-2.8^{+1.4}_{-2.1}$	0.59	4.36	13.7	5
J2007+2722	$0.35^{+0.21}_{-0.19}$	$0.25^{+0.22}_{-0.13}$	$-0.85^{+0.34}_{-0.41}$	0.79	2.74	10.2	2

Note. The peak frequency $\nu_{\rm p}$ is the frequency at which this spectrum displays a maximum flux. The number in the last unmarked column indicates the number of the Figure from this paper in which the spectrum, along with the fitted model, is plotted.
[a] Is not considered as GPS (see Section 3.4).

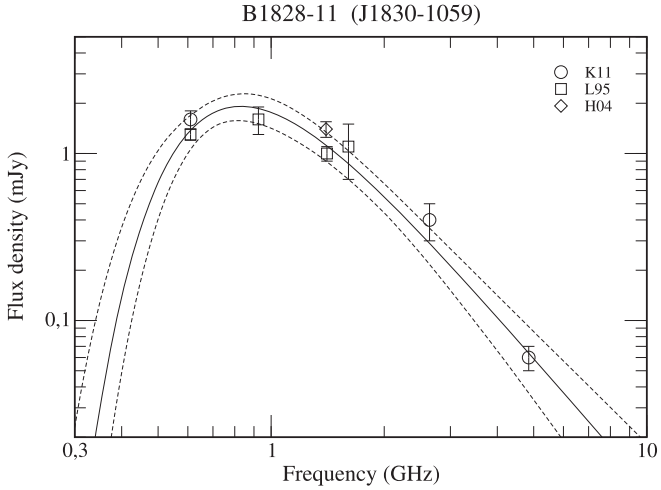

Figure 7. Spectrum of PSR B1828−11. The acronyms are explained in the previous figures. The curve represents our fits to the data using the function given in Equation (1).

occasional discoveries; however, they will be much more time consuming.

4.5. GPS Radio Magnetars

We also included in our studies two radio magnetars, J1550−5418 and J1622−4950, that were previously reported by Kijak et al. (2013) to exhibit GPS-type spectra, with apparent peaks at very high frequencies. Another case was studied by Lewandowski et al. (2015c), namely the Sgr A* radio magnetar, located very close to the central black hole of our Galaxy. This object was also exhibiting GPS characteristics, which evolved with time—since, according to the model shown by the authors, the amount of absorption was decreasing with time.

One has to note a significant difference between our results and the study of the Sgr A* magnetar: the spectra that were analyzed for this object were obtained for individual epochs, while the spectra we show here for J1550−5418 and J1622−4950 were obtained from all available radio flux density measurements regardless of the date of observations. Therefore a certain degree of caution is required when interpreting the results. If the radio spectra of the magnetars indeed change over time, then the spectra we used for our models do not correspond to any given moment in time and their shape may be heavily affected by the actual evolution. For that reason, the physical parameters inferred from the models should be treated only as rough/average estimates.

Kijak et al. (2013) noted that the peak frequencies for the two radio magnetars are much higher than the values obtained for the remaining GPS pulsars, suggesting that the magnetars have to be in even more extreme environments as compared to the other GPS pulsars. This would be explained by the fact that these magnetars are extremely young objects (see Table 4; ages 1410 and 4030 years), which would indicate that one can expect much more extreme conditions in their surroundings, especially when it comes to the electron density. The density influence will be somewhat offset by higher temperatures in these surroundings; however, the much stronger dependence on density (through the EM) would explain higher amounts of absorption and higher peak frequencies. We also have to note that the peak frequencies obtained from our thermal absorption fits are significantly lower than the ones reported before, i.e., 3.27 and 3.7 GHz instead of 5.0 and 8.3 GHz (see also Figure 8). This discrepancy comes from the fact that the previous paper used the purely morphological model of parabolic spectral shape proposed by Kuzmin & Losovsky (2000). The application of the real physical model suggests that the radio magnetars have relatively flat spectra: the intrinsic spectral indexes we obtained from our modeling are the lowest in the sample (−0.46 and −0.54), which combined with the

Table 4
Physical Parameters of Absorbers Derived from Thermal Absorption Model Fits, Along with Basic Relevant Pulsar/Magnetar Parameters (Taken from the ATNF Catalog)

PSR	DM (pc cm^{-3})	Age (kyr)	Size (pc)	n_e (cm^{-3})	EM (10^4 pc cm^{-6})	T (K)	Remarks	
B1054−62	320	1870	0.1	1601 ± 3	25.648 ± 0.096	5080^{+18100}_{-3780}	H II (BBW 328)	
			1.0	160.1 ± 0.3	2.56648 ± 0.0096	923^{+3282}_{-686}		5
			10.0	16.01 ± 0.03	0.25648 ± 0.00096	179^{+596}_{-125}		
J1550−5418	830	1.41	0.1	4150 ± 250	172.2 ± 20.8	3210^{+2710}_{-2030}	Radio magnetar	
			1.0	415 ± 25	17.22 ± 2.08	583^{+493}_{-369}	SNR	6
			10.0	41.5 ± 2.5	1.7222 ± 0.208	106^{+90}_{-67}		
J1622−4950	820	4.03	0.1	4100 ± 150	168.1 ± 12.3	2280^{+1460}_{-1060}	Radio magnetar	
			1.0	410 ± 15	16.81 ± 1.23	414^{+265}_{-193}	SNR, PWN?, H II	6
			10.0	41.0 ± 1.5	1.681 ± 0.123	75^{+48}_{-35}		
B1641−45	479	359	0.1	2394 ± 4	57.31 ± 0.19	5413^{+1040}_{-922}	HESS	
			1.0	239.4 ± 0.4	5.731 ± 0.019	983^{+190}_{-167}	(near Westerlund 1	1
			10.0	23.94 ± 0.004	0.57 ± 0.0019	179^{+34}_{-30}	globular cluster)	
J1723−3659	254	401	0.1	1271.0 ± 1.5	16.154 ± 0.038	3150^{+172}_{-153}		
			1.0	127.10 ± 0.15	1.6154 ± 0.0038	572^{+31}_{-28}		1
			10.0	12.710 ± 0.015	0.16154 ± 0.00038	$103.9^{+5.7}_{-5.0}$		
J1809−1917	197	51.3	0.1	986 ± 2	9.712 ± 0.039	267^{+36}_{-36}	X: bow shock PWN	
			1.0	98.55 ± 0.2	0.9712 ± 0.0039	$48.5^{+6.6}_{-6.6}$	SNR?, H II?, HESS	5
			10	9.855 ± 0.02	0.09712 ± 0.00039	$8.8^{+1.2}_{-1.2}$		
B1822−14	357	195	0.1	1785 ± 25	31.86 ± 0.89	10100^{+4130}_{-3590}	SNR, H II	
			1.0	178.5 ± 2.5	3.186 ± 0.089	1830^{+751}_{-652}		2
			10.0	17.85 ± 0.25	0.3186 ± 0.0089	332^{+136}_{-118}		
B1823−13	231	21.4	0.1	1155 ± 5	13.34 ± 0.12	2670^{+3250}_{-1070}	X: PWN	
			1.0	115.5 ± 0.5	1.334 ± 0.012	485^{+589}_{-194}	HESS	2
			10.0	11.55 ± 0.05	0.1334 ± 0.0012	88^{+107}_{-35}		
B1828−11	161	107	0.1	808 ± 1	6.52 ± 0.016	660^{+150}_{-144}		
			1.0	80.8 ± 0.1	0.6521 ± 0.0016	120^{+27}_{-26}		7
			10.0	8.08 ± 0.01	0.06521 ± 0.00016	$21.6^{+4.9}_{-4.8}$		
J1835−1020	114	810	0.1	568.5 ± 4.5	3.232 ± 0.051	988^{+89}_{-86}		
			1.0	56.85 0.45	0.3232 ± 0.0051	180^{+16}_{-16}		1
			10.0	5.685 ± 0.045	0.03232 ± 0.0051	$32.6^{+2.9}_{-2.8}$		
J1841−0345	194	55.9	0.1	971.6 ± 0.3	9.4401 ± 0.0058	3960^{+1340}_{-1080}	H II?	
			1.0	97.16 ± 0.03	0.94401 ± 0.00058	720^{+244}_{-196}		1
			10.0	9.716 ± 0.003	0.094401 ± 0.000058	131^{+44}_{-36}		
J1852−0635	171	567	0.1	855 ± 30	7.31 ± 0.51	1670^{+1813}_{-713}		
			1.0	85.5 ± 3.0	0.731 ± 0.051	303^{+329}_{-129}		2
			10.0	8.55 ± 0.30	0.0731 ± 0.0051	$55.1^{+59.8}_{-23.5}$		
J1901+0510	429	313	0.1	2145 ± 35	46.0 ± 1.5	7560^{+937}_{-780}		
			1.0	21.45 ± 3.5	4.60 ± 0.15	1370^{+170}_{-145}		1
			10.0	21.45 ± 0.35	0.460 ± 0.015	249^{+31}_{-26}		

Table 4
(Continued)

PSR	DM (pc cm^{-3})	Age (kyr)	Size (pc)	n_e (cm^{-3})	EM (10^4 pc cm^{-6})	T (K)	Remarks	
J1907+0918	358	38	0.1	1789.5 ± 0.5	32.023 ± 0.018	3520^{+3900}_{-2080}	SNR?	
			1.0	178.95 ± 0.5	3.2023 ± 0.0018	639^{+711}_{-377}		5
			10.0	17.895 ± 0.05	0.32023 ± 0.00018	116^{+129}_{-68}		
J2007+2722	127	404000	0.1	635 ± 2	4.032 ± 0.025	1140^{+749}_{-446}		
			1.0	63.5 ± 0.2	0.4032 ± 0.0025	207^{+136}_{-81}		2
			10.0	6.35 ± 0.02	0.04032 ± 0.00025	38^{+25}_{-15}		

Note. The remarks column indicates definite or possible associations of the neutron star with an SNR, a PWN, an H II region, or an unidentified X-ray source from the HESS catalog. The number in the last unmarked column indicates the number of figure in which the spectrum, along with the fitted model, is plotted.

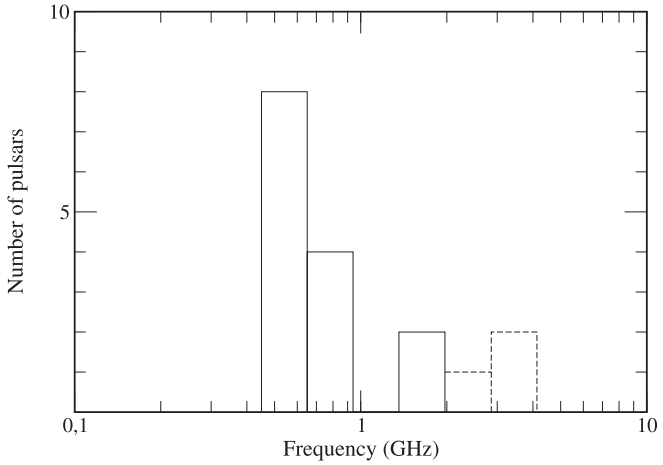

Figure 8. Histogram showing the distribution of GPS pulsar/radio magnetar peak frequencies (see also Table 4). The dashed boxes represent the peak frequencies of radio magnetars.

thermal absorption profile causes only very small changes in the observed flux density over a relatively wide range of frequencies. The use of the actual model moves the peak frequency from the middle of that "almost flat" spectral region toward lower frequencies, yielding the values around 3 GHz. Lewandowski et al. (2015c), in their study of the Sgr A* radio magnetar, obtained a similar value (which can be inferred from their spectra plots), about 3.5 GHz at 40 days since the magnetar outburst. And Pennucci et al. (2015) observed the spectrum of that magnetar; their plots suggest a peak frequency of about 2–2.5 GHz, and their observations were made approximately 100 days after the outburst. All of these studies clearly indicate that if thermal absorption is the cause of the spectral turnovers in radio magnetars, then indeed the parameters of the absorbers must be more extreme than in the case of regular GPS pulsars.

In Section 4.4 we discussed some basic aspects of GPS pulsar searches. Based on that, we believe that the main reason for the fact that we know of magnetars with such high peak frequencies but did not discover pulsars exhibiting such a high amount of absorption is purely due to the discovery bias: the magnetars are discovered in the radio regime only after their initial X-ray outburst discovery (which often provides the rotational parameters as well), while for regular pulsars we do not have that option and we are forced to perform a full search, which (as we discussed above) can succeed only if it is performed at a sufficiently high observing frequency. It is possible that there are pulsars located in similarly extreme environments that simply have not been discovered yet because no one searched for them at observing frequencies around 10 GHz and above.

Moreover, there is a possibility that the reason why some of the magnetars do not exhibit radio emission at all may be due to thermal absorption that is even more extreme than in the cases of J1550−5418 and J1622−4950. However, given the nearly flat intrinsic radio-magnetar spectra, these objects would be easier to find at frequencies around and above 10 GHz, and we know that such attempts were made, at least in some selected cases. Hence we believe that free–free absorption as the explanation for radio-quiet magnetars is not very likely.

5. Summary

We used the interferometric imaging technique to estimate the low radio frequency flux in 15 pulsars. The high sensitivity of the measurements allowed us to construct the spectral shape of these pulsars, and in the process we identified five new pulsars with GPS. In addition, our measurements resulted in tighter constraints on the low-frequency spectra of four pulsars and confirmed their GPS characteristics. To summarize, the GPS pulsar population now consists of 17 sources.

The GPS phenomenon in pulsars is most likely a result of thermal absorption of the pulsar flux in specialized environments along the line of sight. A detailed study was conducted where the low frequency turnover in the spectral shape was successfully modeled using thermal absorption, using a three-parameter fit procedure similar to the one employed by Basu et al. (2016). We presented the results of our modeling for 14 GPS pulsars (see Figures 1, 2, 5, 6). The remaining three GPS neutron stars—PSR B1800−21, PSR B1259−63 in the binary system with Be star LS 2883, and SGR J1745−2900—have been modeled in separate works (see Section 4.4). A detailed study of PSR J1740+1000, a source that was claimed to show GPS characteristics by Dembska et al. (2014), is in progress. The spectral shape arising due to thermal absorption is not sufficient to fully characterize the physical properties like temperature, electron density, and size of the absorbing region. However, using basic physical arguments we have explored the nature of the absorber and ruled out some of the potential candidates.

We also discussed the strategies for finding GPS pulsars in future search surveys. The optimal frequency range is usually a few times larger than the peak frequency, meaning that for a

normal GPS pulsar (with a peak frequency close to 1 GHz) the optimal frequency would be greater than 3 GHz, while for the sources with much stronger absorption, similar to radio magnetars (ν_p close to 3 GHz) the optimal frequency would be much higher, possibly close to 10 GHz. Therefore we believe that a targeted search surveys of known PWNe, H II regions, and SNRs should be the way to go. However, we also have to point out that there is a possibility that a lot of GPS sources still hide in the known pulsar population. Such sources have not been identified yet simply because for the majority of pulsars the shapes of their spectra remain unknown, especially in the low-frequency range (below 1 GHz) where thermal free–free absorption would manifest itself.

We thank the staff of the Giant Metrewave Radio Telescope (GMRT), who have made these observations possible. The GMRT is run by the National Centre for Radio Astrophysics of the Tata Institute of Fundamental Research. This research was partially supported by the grant DEC-2013/09/B/ST9/02177 of the Polish National Science Centre.

References

Allen, B., Knispel, B., Cordes, J. M., et al. 2013, ApJ, 773, 91
Anderson, G. E., Gaensler, B. M., Slane, P. O., et al. 2012, ApJ, 751, 53
Basu, R., Rożko, K., Lewandowski, W., Kijak, J., & Dembska, M. 2016, MNRAS, 458, 2509
Bates, S. D., Johnston, S., Lorimer, D. R., et al. 2011, MNRAS, 411, 1575
Bates, S. D., Lorimer, D. R., & Verbiest, J. P. W. 2013, MNRAS, 431, 1352
Camilo, F., Ransom, S. M., Halpern, J. P., & Reynolds, J. 2007, ApJL, 666, L93
Camilo, F., Reynolds, J., Johnston, S., Halpern, J. P., & Ransom, S. M. 2008, ApJ, 679, 681
Champion, D. J., Lorimer, D. R., McLaughlin, M. A., et al. 2005, MNRAS, 363, 929
Costa, M. E., McCulloch, P. M., & Hamilton, P. A. 1991, MNRAS, 252, 13
Dembska, M., Basu, R., Kijak, J., & Lewandowski, W. 2015a, MNRAS, 449, 1869
Dembska, M., Kijak, J., Koralewska, O., et al. 2015b, Ap&SS, 359, 31
Dembska, M., Kijak, J., Jessner, A., et al. 2014, MNRAS, 445, 3105
Geyer, M., & Karastergiou, A., 2016, MNRAS, 462, 2587
Hobbs, G., Faulkner, A., Stairs, I. H., et al. 2004, MNRAS, 352, 1439
Johnston, S., Karastergiou, A., & Willett, K. 2006, MNRAS, 369, 1916
Keith, M. J., Johnston, S., Levin, L., & Bailes, M. 2011, MNRAS, 416, 346
Kijak, J., Dembska, M., Lewandowski, W., Melikidze, G., & Sendyk, M. 2011a, MNRAS, 418, L114
Kijak, J., Gupta, Y., & Krzeszowski, K. 2007, A&A, 462, 699
Kijak, J., Kramer, M., Wielebinski, R., & Jessner, A. 1998, A&AS, 127, 153
Kijak, J., Lewandowski, W., Maron, O., Gupta, Y., & Jessner, A. 2011b, A&A, 531, A16
Kijak, J., & Maron, O. 2004, in IAU Symp, 218, Young Neutron Stars and Their Environments, ed. F. Camilo & B. M. Gaensler (San Francisco, CA: ASP), 339
Kijak, J., Tarczewski, L., Lewandowski, W., & Melikidze, G. 2013, ApJ, 772, 29
Krishnakumar, M. A., Mitra, D., Naidu, A., Joshi, B. C., & Manoharan, P. K. 2015, ApJ, 804, 23
Kuzmin, A. D., & Losovsky, B. Ya. 2000, AstL, 26, 500
Levin, L., Bailes, M., Bates, S., et al. 2010, ApJL, 721, L33
Levin, L., Bailes, M., Bates, S. D., et al. 2012, MNRAS, 422, 2489
Lewandowski, W., Dembska, M., Kijak, J., & Kowalińska, M. 2013, MNRAS, 434, 69
Lewandowski, W., Kowalinska, M., & Kijak, J. 2015a, MNRAS, 449, 1570
Lewandowski, W., Rożko, K., Kijak, J., Bhattacharyya, B., & Roy, J. 2015b, MNRAS, 454, 2517
Lewandowski, W., Rożko, K., Kijak, J., & Melikidze, G. I. 2015c, ApJ, 808, 18
Lorimer, D. R., & Xilouris, K. M. 2000, ApJ, 545, 385L
Lorimer, D. R., Yates, J. A., Lyne, A. G., & Gould, D. M. 1995, MNRAS, 273, 411
Manchester, R. N., Hobbs, G. B., Teoh, A., & Hobbs, M. 2005, AJ, 129, 1993
Manchester, R. N., Lyne, A. G., Camilo, F., et al. 2001, MNRAS, 328, 17
Manchester, R. N., Lyne, A. G., Taylor, J. H., et al. 1978, MNRAS, 185, 09
Maron, O., Kijak, J., Kramer, M., & Wielebinski, R. 2000, A&AS, 147, 195
Morris, D. J., Hobbs, G., Lyne, A. G., et al. 2002, MNRAS, 335, 275
Pennucci, T. T., Possenti, A., Esposito, P., et al. 2015, ApJ, 808, 81
Perley, R. A., & Butler, B. J. 2013, ApJS, 204, 19
Rajwade, K., Lorimer, D., & Anderson, L. 2016a, arXiv:1611.06977
Rajwade, K., Lorimer, D. R., & Anderson, L. D. 2016b, MNRAS, 455, 493
Rybicki, G. B., & Lightman, A. P. 1979, Radiative Processes in Astrophysics (New York: Wiley)
Sieber, W. 1973, A&A, 28, 237
Taylor, J. H., Manchester, R. N., & Lyne, A. G. 1993, ApJS, 88, 529
van Ommen, T. D., D'Alessandro, F., Hamilton, P. A., & McCulloch, P. M. 1997, MNRAS, 287, 307
Wilson, T. L., Rohlfs, K., & Hüttemeister, S. 2009, Tools of Radio Astronomy (Berlin: Springer)
Wu, X., Manchester, R. N., Lyne, A. G., & Qiao, G. 1993, MNRAS, 261, 630